

# Bipolar Tetraarylsilanes as Universal Hosts for Blue, Green, Orange, and White Electrophosphorescence with High Efficiency and Low Efficiency Roll-Off

Shaolong Gong, Yonghua Chen, Jiajia Luo, Chuluo Yang,\* Cheng Zhong, Jingui Qin, and Dongge Ma\*

A series of tetraarylsilane compounds, namely *p*-BISiTPA (1), *m*-BISiTPA (2), *p*-OXDSiTPA (3), *m*-OXDSiTPA (4), are designed and synthesized by incorporating electron-donating arylamine and electron-accepting benzimidazole or oxadiazole into one molecule via a silicon-bridge linkage mode. Their thermal, photophysical and electrochemical properties can be finely tuned through the different groups and linking topologies. The *para*-disposition compounds 1 and 3 display higher glass transition temperatures, slightly lower HOMO levels and triplet energies than their *meta*-disposition isomers 2 and 4, respectively. The silicon-interrupted conjugation of the electron-donating and electron-accepting segments gives these materials the following advantages: i) relative high triplet energies in the range of 2.69–2.73 eV; ii) HOMO/LUMO levels of the compounds mainly depend on the electron-donating and electron-accepting groups, respectively; iii) bipolar transporting feature as indicated by hole-only and electron-only devices. These advantages make these materials ideal universal hosts for multicolor phosphorescent OLEDs. 1 and 3 have been demonstrated as universal hosts for blue, green, orange and white electrophosphorescence, exhibiting high efficiencies and low efficiency roll-off. For example, the devices hosted by 1 achieve maximum external quantum efficiencies of 16.1% for blue, 22.7% for green, 20.5% for orange, and 19.1% for white electrophosphorescence. Furthermore, the external quantum efficiencies are still as high as 14.2% for blue, 22.4% for green, 18.9% for orange, and 17.4% for white electrophosphorescence at a high luminance of 1000 cd m<sup>-2</sup>. The two-color, all-phosphor white device hosted by 3 acquires a maximum current efficiency of 51.4 cd A<sup>-1</sup>, and a maximum power efficiency of 51.9 lm W<sup>-1</sup>. These values are among the highest for single emitting layer white PhOLEDs reported till now.

## 1. Introduction

Phosphorescent organic light-emitting diodes (PhOLEDs) have attracted intense interest because they can approach 100% internal quantum efficiency by utilizing both singlet and triplet excitons.<sup>[1–3]</sup> Recently, green and red PhOLEDs with 100% internal quantum efficiency have been reported,<sup>[4–6]</sup> but highly efficient and stable blue PhOLEDs have yet to be developed. Furthermore, the low efficiency and instability of blue PhOLEDs has become a bottleneck in the development of efficient and stable white PhOLEDs. To achieve highly efficient electrophosphorescence, phosphorescent emitters of heavy-metal complexes are usually doped into a suitable host material by reducing competitive factors such as concentration quenching and triplet-triplet annihilation.<sup>[7]</sup> Given this, a universal host for blue, green, and red phosphors is vital for the realization of white PhOLEDs. However, the design of such universal host is a considerable challenge. As a host for blue phosphor, its triplet energy level must be larger than photon energies of blue light ( $\geq 2.7$  eV) to maintain effective exothermic energy transfer from host to guest.<sup>[8]</sup> On the other hand, as a host for green or red phosphor, a triplet energy higher than blue phosphor may not be desirable because a high triplet energy generally signifies a large electrical bandgap, i.e., a low-lying highest occupied molecular orbital (HOMO) and/or high-lying lowest occupied molecular orbital (LUMO) level, which may cause large energy barriers between adjacent layers.<sup>[9]</sup> Therefore, in a universal host for blue, green, and red phosphors, a compromise must be reached between high triplet energy and appropriate HOMO/LUMO levels.

Carbazole-based compounds have been widely utilized as the host materials for blue PhOLEDs.<sup>[10,11]</sup> Additionally, tetraarylsilane compounds with ultrahigh singlet ( $\sim 4.5$  eV) and triplet ( $\sim 3.5$  eV) energies have been reported as host materials for deep blue electrophosphorescence,<sup>[12]</sup> but their poor charge-transporting ability and very high hole-injection barrier hamper their further

S. Gong, J. Luo, Prof. C. Yang, C. Zhong, Prof. J. Qin  
Department of Chemistry  
Hubei Key Lab on Organic and Polymeric Optoelectronic Materials  
Wuhan University  
Wuhan 430072, People's Republic of China  
E-mail: clyang@whu.edu.cn

Y. Chen, Prof. D. Ma  
State Key Laboratory of Polymer Physics and Chemistry  
Changchun Institute of Applied Chemistry  
Chinese Academy of Sciences  
Changchun 130022, People's Republic of China  
E-mail: mdg1014@ciac.jl.cn

DOI: 10.1002/adfm.201002066

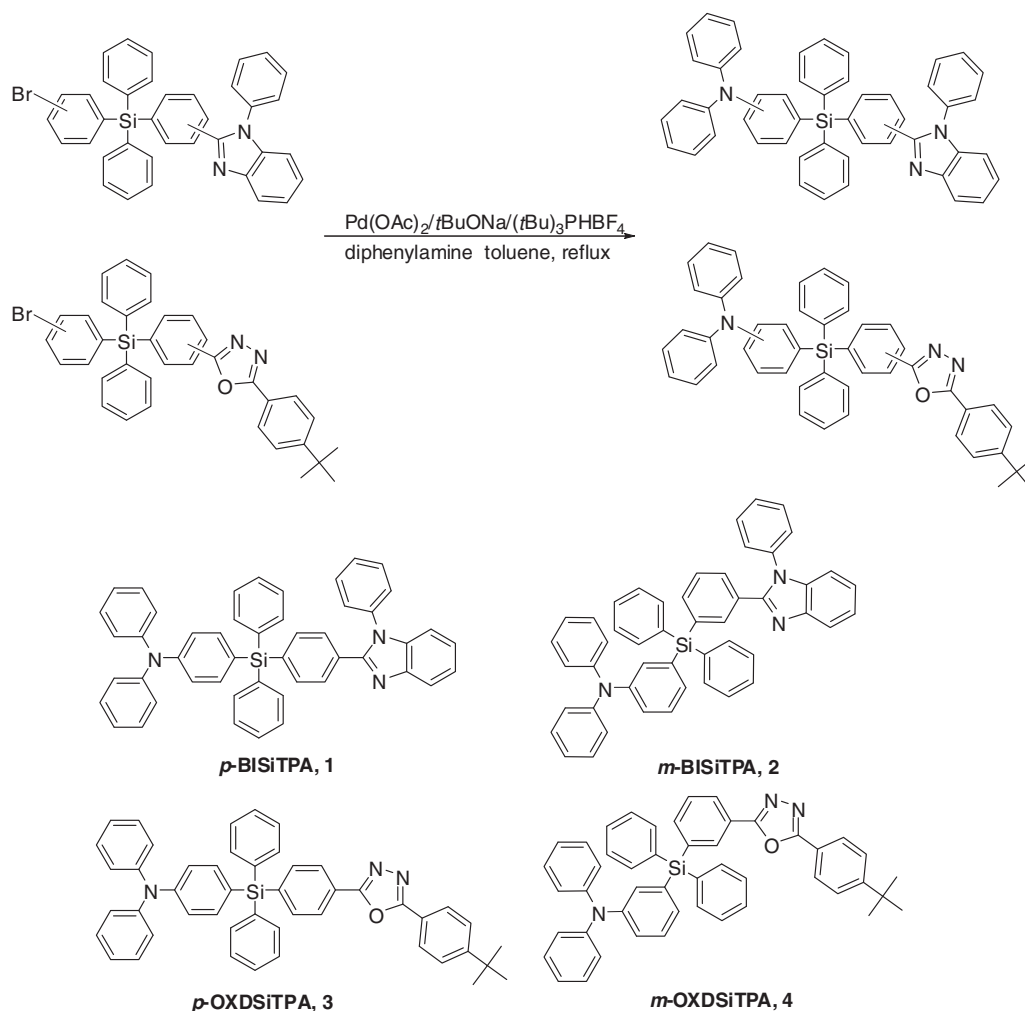
usage as host materials. To reduce the hole-injection barrier, p-type tetraarylsilane compounds synthesized by introducing the carbazole moiety have been recently reported as hosts for blue PhOLEDs.<sup>[13,14]</sup> Unfortunately, problems still remain in terms of low efficiency and large efficiency roll-off due to the imbalance of carrier injection and transport. To address this issue, a bipolar host can play an important role because it could facilitate the balanced transport of both hole and electron, and broaden the exciton-formation zone, consequently improving the device performance and reduce efficiency roll-off.<sup>[15,16]</sup> In this context, we designed and synthesized a series of tetraarylsilane compounds by integrating electron-donating arylamine and electron-accepting benzimidazole or oxadiazole into one molecule. We anticipate that the electron-donating and electron-accepting moieties would impart the material with bipolar transporting characteristics; meanwhile, the whole molecule would maintain relative high triplet energy owing to silicon-interrupted conjugation of two segments. We also expect that different groups and linking modes of the electron-donor and electron-acceptor would finely tune their photophysical and electrochemical properties, and consequently modulate their triplet energies and HOMO/LUMO levels to some extent. We

will present a comprehensive investigation that encompasses the thermal, photophysical, and electrochemical properties of the compounds as well as the theoretical modeling, and demonstrate the applicability of these materials as universal hosts for blue, green, and orange phosphors, and finally for all-phosphor white OLEDs.

## 2. Results and Discussion

### 2.1. Synthesis and Characterization

The synthetic routes and chemical structures of the compounds, (4-{diphenyl[4-(1-phenyl-1*H*-benzimidazol-2-yl)phenyl]silyl}phenyl)diphenylamine (*p*-BISiTPA, **1**), (3-{diphenyl[3-(1-phenyl-1*H*-benzimidazol-2-yl)phenyl]silyl}phenyl)diphenylamine (*m*-BISiTPA, **2**), {4-[[4-[5-(4-*tert*-butylphenyl)-1,3,4-oxadiazol-2-yl]phenyl](diphenyl)silyl]phenyl}diphenylamine (*p*-OXDSiTPA, **3**), {3-[[3-[5-(4-*tert*-butylphenyl)-1,3,4-oxadiazol-2-yl]phenyl](diphenyl)silyl]phenyl}diphenylamine (*m*-OXDSiTPA, **4**), are depicted in **Scheme 1**. The electron-withdrawing benzimidazole or oxadiazole moiety was



**Scheme 1.** Synthesis and molecular structures of 1–4.

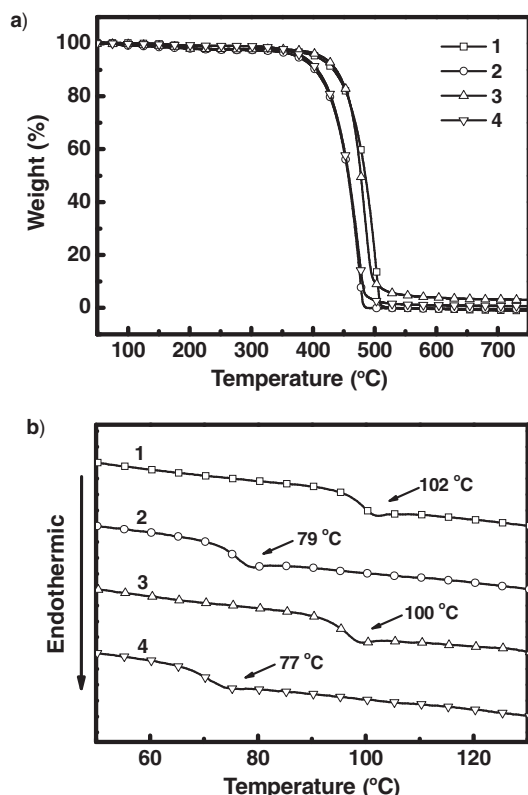


**Figure 1.** a) TGA thermograms of 1–4 recorded at a heating rate of 10 °C min<sup>-1</sup>. b) DSC traces of 1–4 recorded at a heating rate of 10 °C min<sup>-1</sup>.

firstly introduced to the silicon-containing skeleton, and then the electron-donating diphenylamine segment was connected to the skeleton through the palladium-catalyzed C–N coupling reaction of the corresponding bromide intermediates with diphenylamine in good yields (72–80%).<sup>[17]</sup> For 1 and 3, the electron-donor and acceptor units locate at the *para*-disposition of the silicon, while for 2 and 4, the two units situate in the *meta*-disposition of the silicon. The chemical structures of all of the compounds were fully characterized by <sup>1</sup>H NMR and <sup>13</sup>C NMR spectroscopy, mass spectrometry, and elemental analysis (see the Experimental Section).

## 2.2. Thermal Properties

The thermal properties of the compounds were investigated by thermogravimetric analysis (TGA) and differential scanning calorimetry (DSC) (Figure 1 and Table 1). The four compounds

exhibit high thermal decomposition temperatures ( $T_d$ , corresponding to 5% weight loss) in the range of 376–415 °C. Their glass-transition temperatures ( $T_g$ ) range from 77 to 102 °C, which are substantially higher than those of tetraarylsilane compounds (26–53 °C),<sup>[12]</sup> indicating that the introduction of benzimidazole or oxadiazole moiety improves their morphological stability. Additionally, 1 and 3 with a *para*-disposition linkage show significantly higher  $T_g$  values than 2 and 4 with a *meta*-disposition connection.

## 2.3. Photophysical Properties

Figure 2 shows the electronic absorption and fluorescence spectra of the compounds in dilute toluene and CH<sub>2</sub>Cl<sub>2</sub> solution. The absorption peaks around 300 nm for all compounds are consistent with the triphenylamine-centered  $\pi$ – $\pi^*$  transition. In addition, no charge transfer absorption band from the electron-donating triphenylamine to the electron-withdrawing benzimidazole or oxadiazole group can be observed,<sup>[18]</sup> indicating the disruption of the  $\pi$ -conjugation between the two parts owing to the silicon-bridge linkage mode.

The four compounds show emission peaks in the range of 372–408 nm in low-polarity toluene solution. In more polar CH<sub>2</sub>Cl<sub>2</sub> solution, all of the compounds display pronounced dual emission bands simultaneously (Figure 2b): the emission peaks in the range of 358–387 nm can be assigned to the  $\pi$ – $\pi^*$  transitions; the emissions at longer wavelengths around 450–506 nm originate from donor–acceptor charge transfer transitions.<sup>[19]</sup> The charge transfer transitions of 2 and 4 are partially blocked due to the *meta*-disposition linkage, which results in the blue-shifts of the charge transfer bands with respect to the *para*-disposition isomers 1 and 3, respectively. Moreover, the charge transfer emission shift between 1 and 2 is smaller than that between 3 and 4, since the benzimidazole unit in 1 and 2 is a weaker electron-accepting unit than the oxadiazole unit in 3 and 4. Their phosphorescence spectra were measured in a frozen 2-methyltetrahydrofuran matrix at 77 K (Figure 3), and the triplet energy levels were estimated from the highest-energy vibronic sub-band of the phosphorescence spectra. All of the compounds show higher triplet energy levels (2.69 eV for 1, 2.73 eV for 2, 2.70 eV for 3, and 2.72 eV for 4) than that of blue phosphor iridium(III) bis(4,6-(difluorophenyl)pyridine-*N,C*2) picolinate (FIrpic, 2.65 eV),<sup>[20]</sup> which implies they could serve as host materials for the blue triplet emitter.

**Table 1.** Physical data of 1–4.

Compound	$T_g^a$ (°C)	$T_d^b$ (°C)	$\lambda_{abs}^c$ (nm)	$\lambda_{em, max}^c$ (nm)	$\lambda_{abs}^d$ (nm)	$\lambda_{em, max}^d$ (nm)	HOMO/LUMO <sub>exp</sub> <sup>e</sup> (eV)	HOMO/LUMO <sub>cal</sub> <sup>f</sup> (eV)	$E_T^g$ (eV)
1	102	405	308	372	306	363, 473	5.27/NA	5.22/1.78	2.69
2	79	376	301	380	301	387, 450	5.25/NA	5.11/1.70	2.73
3	100	415	299	408	298	359, 506	5.30/2.34	5.30/2.18	2.70
4	77	384	295	393	294	358, 474	5.25/2.26	5.09/2.12	2.72

<sup>a</sup>) Obtained from DSC measurements; <sup>b</sup>) Obtained from TGA measurements; <sup>c</sup>) Measured in toluene; <sup>d</sup>) Measured in CH<sub>2</sub>Cl<sub>2</sub>; <sup>e</sup>) Determined from the onset of oxidation/reduction potentials; <sup>f</sup>) Values from DFT calculation; <sup>g</sup>) Measured in 2-methyltetrahydrofuran at 77 K.

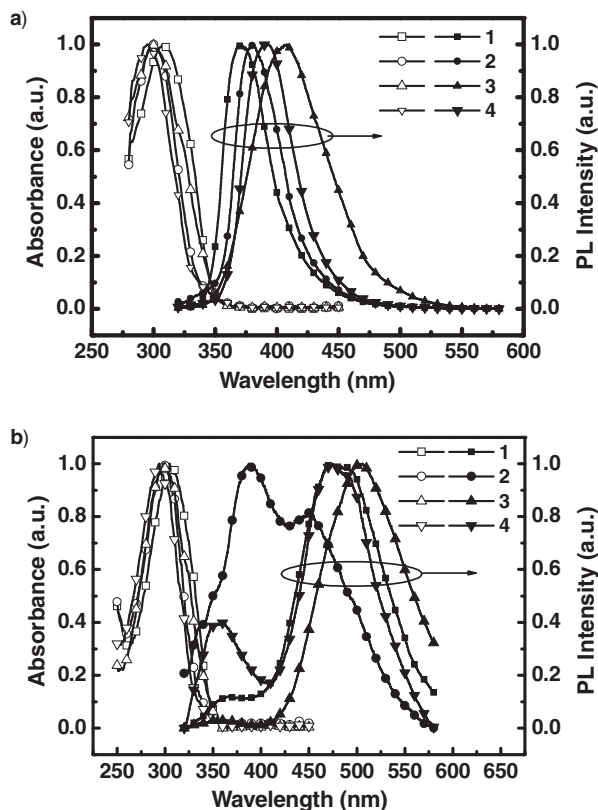


**Figure 2.** UV-vis absorption and PL spectra of 1–4 in a) toluene solution at  $5 \times 10^{-6}$  M and b)  $\text{CH}_2\text{Cl}_2$  solution at  $5 \times 10^{-6}$  M.

#### 2.4. Electrochemical Properties

Cyclic voltammetry (CV) was performed to investigate the electrochemical properties of the compounds (Figure 4). During the anodic scan in dichloromethane, the four compounds all exhibit one quasi-reversible, one-electron oxidation process, which can be assigned to the oxidation of the arylamine moiety.<sup>[21]</sup> Upon cathodic sweeping in THF, 3 and 4 exhibit reversible reduction waves (Figure 4b), arising from the reduction of the n-type oxadiazole segments;<sup>[4b]</sup> while 1 and 2 exhibit no reduction wave.

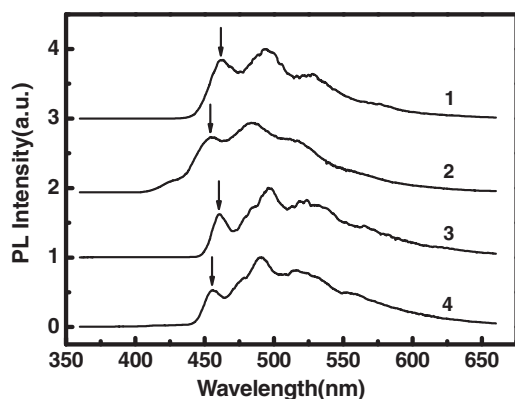


**Figure 3.** The phosphorescence spectra of 1–4 in a frozen 2-methyltetrahydrofuran matrix at 77 K.

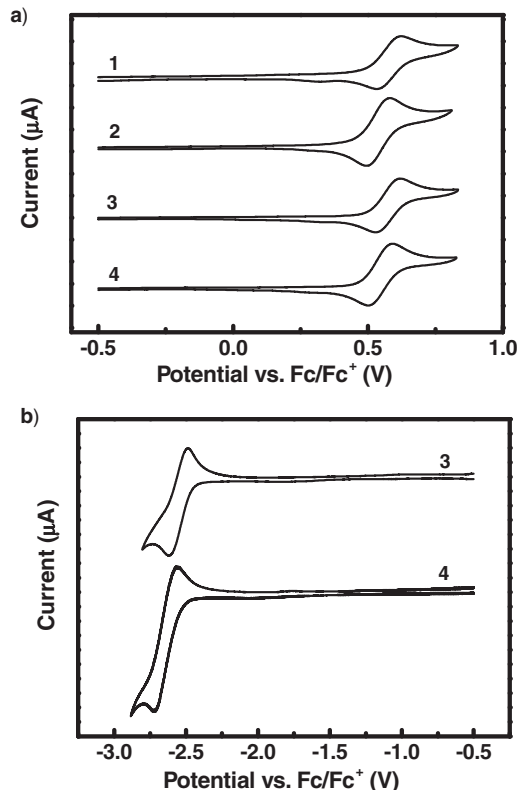


**Figure 4.** Cyclic voltammograms of 1–4 in a)  $\text{CH}_2\text{Cl}_2$  for oxidation and b) THF for reduction.

The HOMO/LUMO energy levels were estimated from the onsets of the oxidation and reduction potentials with regard to the energy level of ferrocene (4.8 eV below vacuum), respectively (Table 1). The four compounds exhibit similar HOMO levels (5.25–5.30 eV), which are much higher than the  $\sim 7.0$  eV of the tetraarylsilane compounds previously reported,<sup>[12]</sup> and even higher than that of widely used hole transporting material 1, 4-bis[(1-naphthylphenyl)amino]biphenyl (NPB, 5.4 eV).<sup>[22]</sup> The LUMO level of 4 (2.26 eV) is slightly higher than that of 3 (2.34 eV), which could be attributed to the different linking modes.

#### 2.5. Theoretical Calculations

To understand the structure-property relationship of the compounds at the molecular level, the geometry were optimized at B3LYP/6–31G(d) level, and the electronic properties of the compounds were calculated at  $\tau$ -HCTHhyb/6–311++G(d, p) level (for details, see the Experimental Section). According to DFT calculations, the HOMO orbitals are mainly located on the electron-donating triphenylamine moiety, while the LUMO orbitals are mainly distributed on the electron-accepting benzimidazole or oxadiazole moiety (Figure 5). All of the compounds have almost complete separation of the HOMO and LUMO at hole- and electron-transporting moieties, which can be rationalized by the disruption of the  $\pi$ -conjugation between the electron-donating and

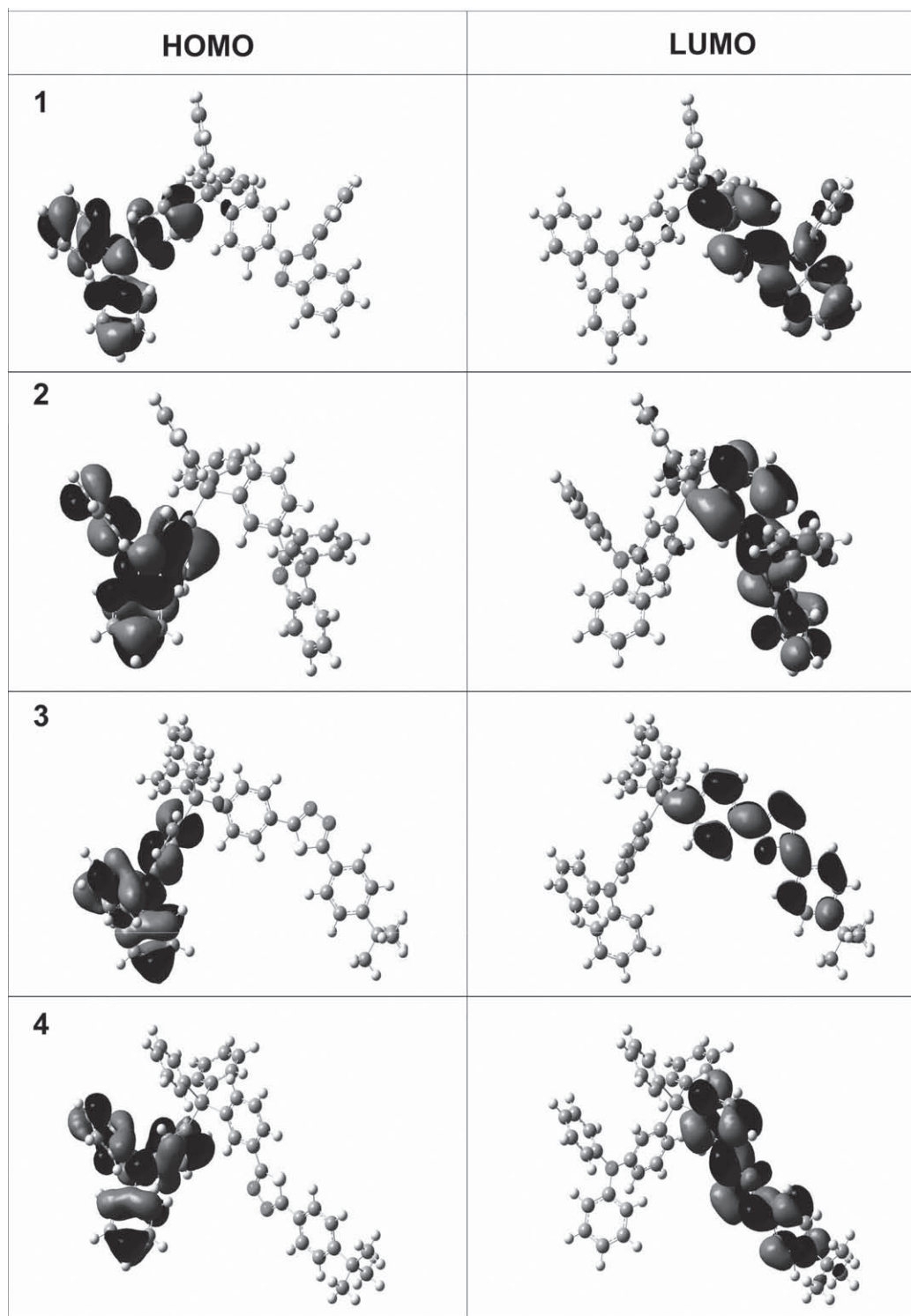
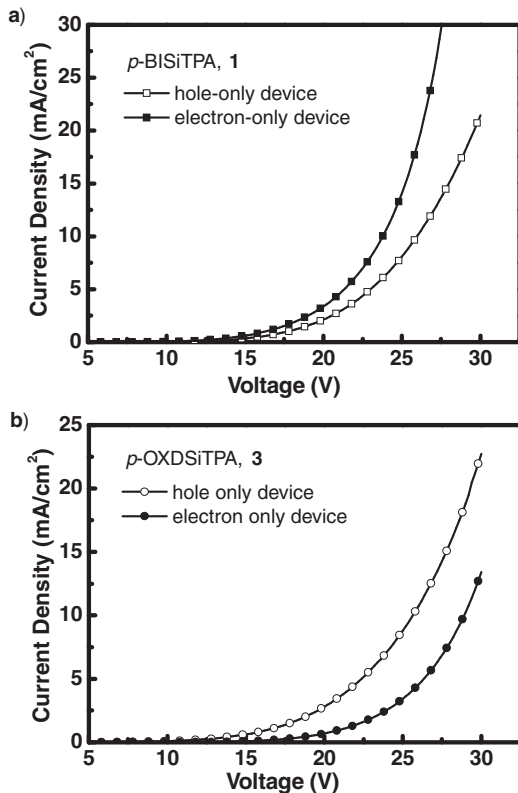


Figure 5. Calculated spatial distributions of the HOMO and LUMO levels of 1–4.

electron-accepting moiety. The complete separation is preferable for efficient hole- and electron-transporting properties, and the prevention of reverse energy transfer.<sup>[23]</sup> The calculated HOMO/LUMO values are in the range of 5.09–5.30/1.70–2.18 eV, which correlate with the experimental data (Table 1).

## 2.6. Electroluminescent Devices

To evaluate the bipolar character of the compounds, we fabricated hole-only devices with the structure of ITO/MoO<sub>3</sub> (10 nm)/NPB (80 nm)/4,4',4''-tri(*N*-carbazolyl)triphenylamine



**Figure 6.** Current density versus voltage characteristics of the hole-only and electron-only devices for a) 1 and b) 3.

(TCTA, 5 nm)/1 or 3 (20 nm)/1,3,5-tris(*N*-phenylbenzimidazol-2-yl)benzene (TPBI, 40 nm)/MoO<sub>3</sub> (40 nm)/Al (100 nm) and electron-only devices with the configuration of ITO/TPBI (40 nm)/NPB (80 nm)/TCTA (5 nm)/1 or 3 (20 nm)/TPBI (40 nm)/LiF (1 nm)/Al (100 nm). For the hole-only devices, most of the electrons can be impeded and only holes can be injected from the anode to the organic layer, because of the large energy injection barrier between the MoO<sub>3</sub> (LUMO = 2.3 eV) and Al (4.3 eV) layers. In the case of the electron-only devices, the TPBI layer, which has a low-lying HOMO level of 6.2 eV, was used to prevent hole-injection from the ITO anode (4.8 eV) to the organic layers. **Figure 6a** and **6b** show current density versus voltage curves of the devices for 1 and 3, respectively. It is obvious that the two compounds are capable of transporting both electron and hole, and exhibit bipolar transporting nature.

We initially examined the performance of FIrpic-based blue phosphorescent devices (devices A–D) with the structures of ITO/MoO<sub>3</sub> (10 nm)/NPB (80 nm)/TCTA (5 nm)/host 1–4: FIrpic (8 wt%, 20 nm)/TPBI (40 nm)/LiF (1 nm)/Al (100 nm). NPB and TPBI were used as the hole- and electron-transporting layers, respectively; TCTA was used as electron/exciton-blocking layer; MoO<sub>3</sub> and LiF served as hole- and electron-injecting layer, respectively; FIrpic doped in host 1–4 was used as the emitting layer, respectively. **Figure 7** depicts the relative energy levels of the materials employed in the devices. **Figure 8** shows the current density–voltage–brightness (*J–V–L*) characteristics and efficiency versus current density curves for the devices, and the EL data are summarized in **Table 2**. Device B hosted by

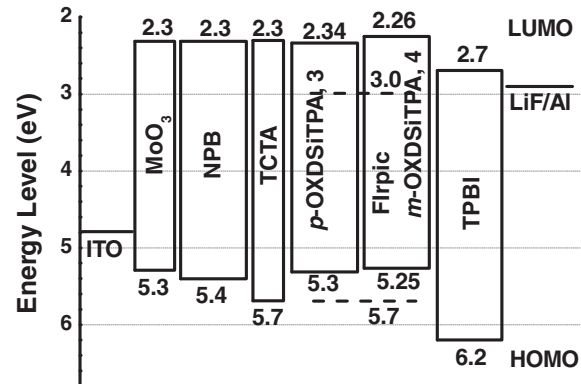


**Figure 7.** Energy level diagrams for devices C and D.

*meta*-disposition 2 achieves a maximum current efficiency ( $\eta_{c,max}$ ) of 31.4 cd A<sup>-1</sup>, a maximum power efficiency ( $\eta_{p,max}$ ) of 21.0 lm W<sup>-1</sup> and a maximum external quantum efficiency ( $\eta_{ext,max}$ ) of 14.6%. In comparison, device A using *para*-disposition 1 as the host exhibits higher performance with  $\eta_{c,max}$  of 35.1 cd A<sup>-1</sup>,  $\eta_{p,max}$  of 26.1 lm W<sup>-1</sup>, and  $\eta_{ext,max}$  of 16.1%. The same trend can be observed for devices C and D. Device C hosted by *para*-disposition 3 displays substantially higher efficiencies ( $\eta_{c,max}$  of 36.9 cd A<sup>-1</sup>,  $\eta_{p,max}$  of 31.4 lm W<sup>-1</sup>, and  $\eta_{ext,max}$  of 14.5%) than device D hosted by *meta*-disposition 4 ( $\eta_{c,max}$  of 26.7 cd A<sup>-1</sup>,  $\eta_{p,max}$

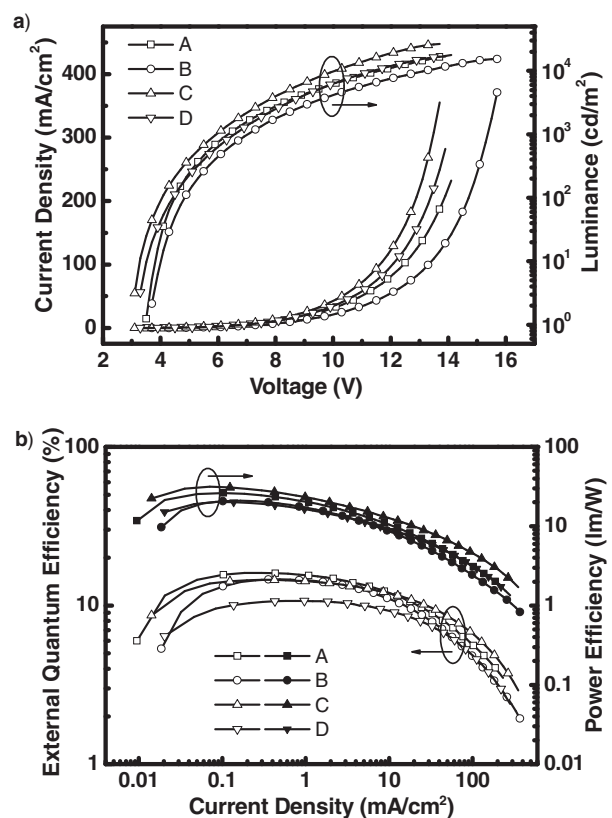


**Figure 8.** a) Current density–voltage–brightness characteristics for devices A–D. b) External quantum efficiency and power efficiency versus current density curves for devices A–D.

**Table 2.** Electroluminescence characteristics of the devices.<sup>a)</sup>

Device	Host/Guest	$V_{on}$ [V]	$L_{max}$ [ $cd\ m^{-2}$ ] ( $V$ at $L_{max}$ , V)	$\eta_c^{b)}$ [ $cd\ A^{-1}$ ]	$\eta_p^{b)}$ [ $lm\ W^{-1}$ ]	$\eta_{ext}^{b)}$ [%]	CIE [x,y] <sup>c)</sup>
A	1/Ir-B	3.5	17798 (14.1)	35.1, 35.1, 31.1	26.1, 24.5, 15.5	16.1, 16.1, 14.2	0.18, 0.32
B	2/Ir-B	3.7	15421 (15.7)	31.4, 31.3, 27.6	21.0, 20.1, 12.2	14.6, 14.6, 12.9	0.17, 0.31
C	3/Ir-B	3.1	26439 (13.7)	36.9, 36.9, 34.4	31.4, 28.3, 18.3	14.5, 14.5, 13.5	0.19, 0.39
D	4/Ir-B	3.3	16870 (13.9)	26.7, 26.5, 25.5	20.3, 18.5, 12.3	10.7, 10.6, 10.2	0.19, 0.38
E	1/Ir-G	3.1	48066 (10.1)	86.9, 84.7, 85.8	72.4, 71.8, 57.3	22.7, 22.1, 22.4	0.35, 0.62
F	2/Ir-G	3.3	47073 (13.3)	70.8, 67.9, 69.7	45.4, 45.4, 35.9	19.3, 18.5, 19.0	0.36, 0.60
G	3/Ir-G	2.7	48331 (10.9)	75.5, 75.3, 74.8	77.8, 71.6, 52.2	19.7, 19.6, 19.5	0.35, 0.62
H	4/Ir-G	2.9	47574 (11.1)	84.2, 81.4, 83.1	70.4, 69.1, 51.2	21.9, 21.2, 21.7	0.35, 0.62
I	1/Ir-O	3.1	47756 (13.1)	57.8, 57.3, 53.2	51.9, 43.9, 29.3	20.5, 20.4, 18.9	0.52, 0.48
J	3/Ir-O	2.9	45417 (12.7)	52.4, 52.3, 50.4	48.7, 44.4, 31.0	17.9, 17.9, 17.2	0.51, 0.49
K	1/Ir-B+Ir-O	3.1	45398 (14.5)	51.8, 51.7, 47.3	42.7, 37.8, 25.2	19.1, 19.1, 17.4	0.38, 0.44
L	3/Ir-B+Ir-O	2.9	35770 (13.9)	51.4, 46.2, 40.4	51.9, 35.4, 22.2	18.3, 16.4, 14.3	0.36, 0.45

<sup>a)</sup>Abbreviations:  $V_{on}$ : turn-on voltage;  $L_{max}$ : maximum luminance;  $V$ : voltage;  $\eta_{ext}$ : external quantum efficiency;  $\eta_c$ : current efficiency;  $\eta_p$ : power efficiency; CIE [x, y]: Commission Internationale de l'Eclairage coordinates; <sup>b)</sup>Order of measured value: maximum, then values at 100 and 1000  $cd\ m^{-2}$ ; <sup>c)</sup>Measured at 7 V.

of 20.3  $lm\ W^{-1}$ , and  $\eta_{ext,max}$  of 10.7%) (Table 2). These values are much higher than those of the comparable blue device using the conventional host of *mCP*, which achieves  $\eta_{c,max}$  of 15.4  $cd\ A^{-1}$ ,  $\eta_{p,max}$  of 10.4  $lm\ W^{-1}$ , and  $\eta_{ext,max}$  of 6.2% (Figure S1). It is worth noting that these devices show a low external quantum efficiency roll-off (Figure 8b). For example, when the brightness reaches 1000  $cd\ m^{-2}$ ,  $\eta_{ext}$  still remains as high as 14.2% with a efficiency roll-off value of 11.8% for device A, and 13.5% with a roll-off value of 6.9% for device C. The Commission Internationale de l'Eclairage (CIE) coordinates vary little for the devices based on the same type of host; however, they vary significantly for the devices based on the different type of host [(0.18, 0.32) for A and (0.17, 0.31) for B; (0.19, 0.39) for C and (0.19, 0.38) for D]. This could be attributed to the recombination zone shift in devices owing to the different charge transporting abilities of the hosts.<sup>[24]</sup>

To test the applicability of the hosts as a green phosphorescent emitter, we fabricated device E-H by using 1–4 as the hosts and 9 wt% iridium(III) bis(2-phenylpyridinato-*N,C^2'*) acetylacetonate [(ppy)<sub>2</sub>Ir(acac)] as the dopant, with an identical device structure as device A. Figure 9 shows the *J-V-L* characteristics and curves of external quantum efficiency and power efficiency versus current density. Excellent performance of green electrophosphorescence can be achieved for devices E-H (Table 2). For example, devices E and H obtain  $\eta_{c,max}$  as high as 86.9  $cd\ A^{-1}$  ( $\eta_{p,max}$  of 72.4  $lm\ W^{-1}$ ,  $\eta_{ext,max}$  of 22.7%) and 84.2  $cd\ A^{-1}$  ( $\eta_{p,max}$  of 70.4  $lm\ W^{-1}$ ,  $\eta_{ext,max}$  of 21.9%), respectively. These values are substantially higher than those of the comparable green device using the host of *mCP* ( $\eta_{c,max}$  of 66.8  $cd\ A^{-1}$ ,  $\eta_{p,max}$  of 59.2  $lm\ W^{-1}$ , and  $\eta_{ext,max}$  of 17.2%, Figure S2). Remarkably, devices E and H still exhibit over 20% external quantum efficiencies (20.6% for device E and 20.1% for device H) at the extremely high luminance of 10 000  $cd\ m^{-2}$ .

To further evaluate the suitability of the compounds as host materials for low energy triplet emitters, we fabricated two orange phosphorescent devices (devices I and J) by using 1 and 3 as the hosts, with the same configuration as device A but using 8 wt% bis(2-(9,9-diethyl-9H-fluoren-2-yl)-1-phenyl-1H-

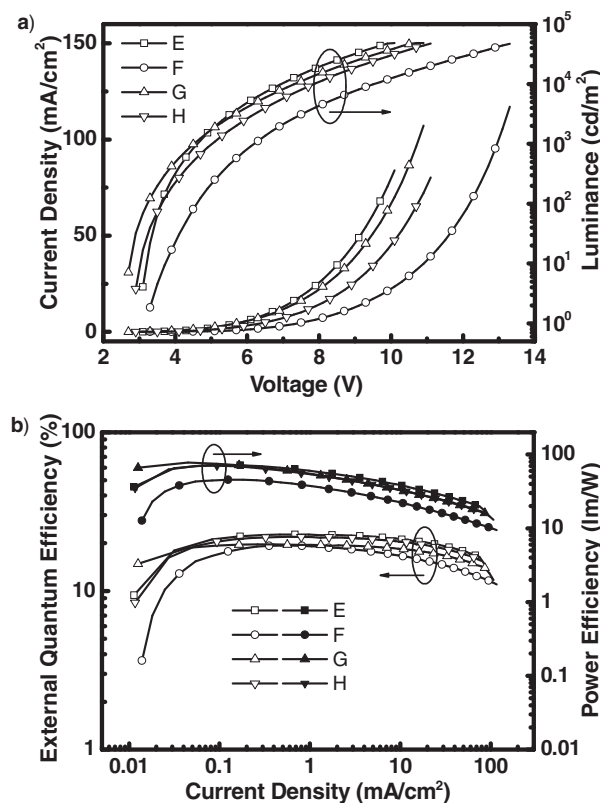


**Figure 9.** a) Current density-voltage-brightness characteristics for devices E-H. b) External quantum efficiency and power efficiency versus current density curves for devices E-H.

benzimidazol-*N,C^3'*iridium acetylacetonate [(fbi)<sub>2</sub>Ir(acac)] as the dopant; these devices achieved better performances for blue electrophosphorescence. The *J-V-L* characteristics and curves of external quantum efficiency and power efficiency versus current density are displayed in Figure 10 with the key parameters summarized in Table 2. The turn-on voltage of

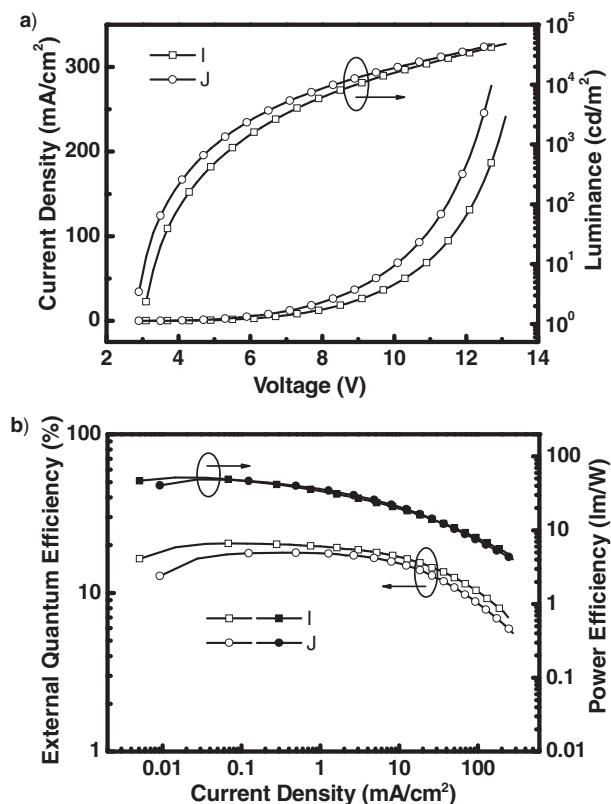


**Figure 10.** a) Current density–voltage–brightness characteristics for devices I and J. b) External quantum efficiency and power efficiency versus current density curves for devices I and J.

device J ( $V_{\text{on}} = 2.9$  V) is lower relative to device I ( $V_{\text{on}} = 3.1$  V). This can be attributed to the low-lying LUMO level of the host **3**, which is better matched with the TPBI layer. Both devices exhibit high performance with a rather low efficiency roll-off at high brightness. For instance, device I exhibits  $\eta_{\text{p,max}}$  of  $51.9 \text{ lm W}^{-1}$ ,  $\eta_{\text{ext,max}}$  of 20.5%, with an external quantum efficiency roll-off of 7.8% at the luminance of  $1000 \text{ cd m}^{-2}$ ; while device J displays  $\eta_{\text{p,max}}$  of  $48.7 \text{ lm W}^{-1}$ ,  $\eta_{\text{ext,max}}$  of 17.9%, with an external quantum efficiency roll-off of 3.9% at the luminance of  $1000 \text{ cd m}^{-2}$ . The devices efficiencies are much higher than those of the comparable orange device hosted by CBP ( $\eta_{\text{c,max}}$  of  $45.0 \text{ cd A}^{-1}$ ,  $\eta_{\text{p,max}}$  of  $31.6 \text{ lm W}^{-1}$ , and  $\eta_{\text{ext,max}}$  of 15.8%, Figure S3), and among the highest for orange PhOLEDs ever reported.<sup>[25]</sup>

In terms of the applicability of the host materials for multicolor triplet emitters, we demonstrated two-color and all-phosphor WOLEDs (devices K and L) with the configuration of ITO/MoO<sub>3</sub> (10 nm)/NPB (80 nm)/TCTA (5 nm)/**1** or **3**: 8 wt% FIrpic: 0.67 wt% (fbi)<sub>2</sub>Ir(acac) (20 nm)/TPBI (40 nm)/LiF (1 nm)/Al (100 nm). FIrpic and (fbi)<sub>2</sub>Ir(acac) were co-doped into the bipolar host **1** or **3** as the single emitting layer. **Figure 11** shows the  $J$ – $V$ – $L$  characteristics and curves of external quantum efficiency and power efficiency versus current density. Device K with **1** as host achieves a maximum brightness of  $45\,398 \text{ cd m}^{-2}$  at 14.5 V,  $\eta_{\text{c,max}}$  of  $51.8 \text{ cd A}^{-1}$ ,  $\eta_{\text{p,max}}$  of  $42.7 \text{ lm W}^{-1}$ , and  $\eta_{\text{ext,max}}$  of 19.1%; these values are

$35\,770 \text{ cd m}^{-2}$  at 13.9 V,  $51.4 \text{ cd A}^{-1}$ ,  $51.9 \text{ lm W}^{-1}$ , and 18.3% for device L with **3** as host. The devices efficiencies are remarkably higher than those of the comparable white device using the conventional host of mCP ( $\eta_{\text{c,max}}$  of  $42.6 \text{ cd A}^{-1}$ ,  $\eta_{\text{p,max}}$  of  $24.3 \text{ lm W}^{-1}$ , and  $\eta_{\text{ext,max}}$  of 14.7%, Figure S4), and among the highest for single emitting layer WOLEDs reported till now.<sup>[26]</sup> Similar to the behavior of the orange devices, device L has a lower turn-on voltage of 2.9 V relative to device K (3.1 V), in consequence, device L exhibits a significantly higher power efficiency than device K. Additionally, both devices K and L exhibit a significantly reduced efficiency roll-off at high brightness compared to our previously reported results under the similar device structures using the conventional host material of mCP,<sup>[26b]</sup> in which  $\eta_{\text{ext}}$  drops to 12.3% with a roll-off value of 36.3% at the luminance of  $1000 \text{ cd m}^{-2}$ ; at the luminance of  $10\,000 \text{ cd m}^{-2}$ ,  $\eta_{\text{ext}}$  declined to only 6.3%. In this work,  $\eta_{\text{ext}}$  of device K at the luminance of  $1000 \text{ cd m}^{-2}$  is still as high as 17.4% with a roll-off value of 8.9%; at the extremely high luminance of  $10\,000 \text{ cd m}^{-2}$ ,  $\eta_{\text{ext}}$  is still 12.2%; while  $\eta_{\text{ext}}$  of device L is 14.3% at  $1000 \text{ cd m}^{-2}$  and 9.7% at  $10\,000 \text{ cd m}^{-2}$ . The high efficiencies and low efficiency roll-off at high luminance for devices K and L can be attributed to the use of the bipolar host which may result in balanced charge fluxes and a broad distribution of recombination regions within the emitting layer. In addition, devices K and L show good color stability (Figure 11c and 11d). When the voltage increases from 8 to 12 V, the CIE coordinates slightly vary from (0.37, 0.43) to (0.36, 0.43) for device K, and from (0.35, 0.45) to (0.34, 0.45) for device L. Affected by the two-color system, the color-rendering index (CRI) of the WOLEDs is not high (67 for device K and 60 for device L).

### 3. Conclusions

In summary, we have developed a new molecular design strategy for bipolar host material by incorporating both electron donor and acceptor into the silicon-bridged structure. The bipolar tetraarylsilane compounds achieve a compromise between a high triplet energy, bipolar transporting nature, and carrier-injection barrier; therefore, these compounds can be utilized as universal host materials for multicolor phosphors. We have successfully fabricated highly efficient blue, green, orange, and white electrophosphorescence by using the tetraarylsilane compounds as host materials. The devices hosted by **1** achieve maximum external quantum efficiencies of 16.1% for blue, 22.7% for green, 20.5% for orange, and 19.1% for white electrophosphorescence. The two-color, all-phosphor white device hosted by **3** acquires a maximum current efficiency of  $51.4 \text{ cd A}^{-1}$ , and a maximum power efficiency of  $51.9 \text{ lm W}^{-1}$ , which are among the highest for single emitting layer white PhOLEDs reported till now. We also note that all the devices exhibit low efficiency roll-off at high luminance. For example, the external quantum efficiencies of devices hosted by **1** are still as high as 14.2% for blue, 22.4% for green, 18.9% for orange and 17.4% for white electrophosphorescence at a high luminance of  $1000 \text{ cd m}^{-2}$ . This can be attributed to the usage of the bipolar tetraarylsilane compounds as hosts.

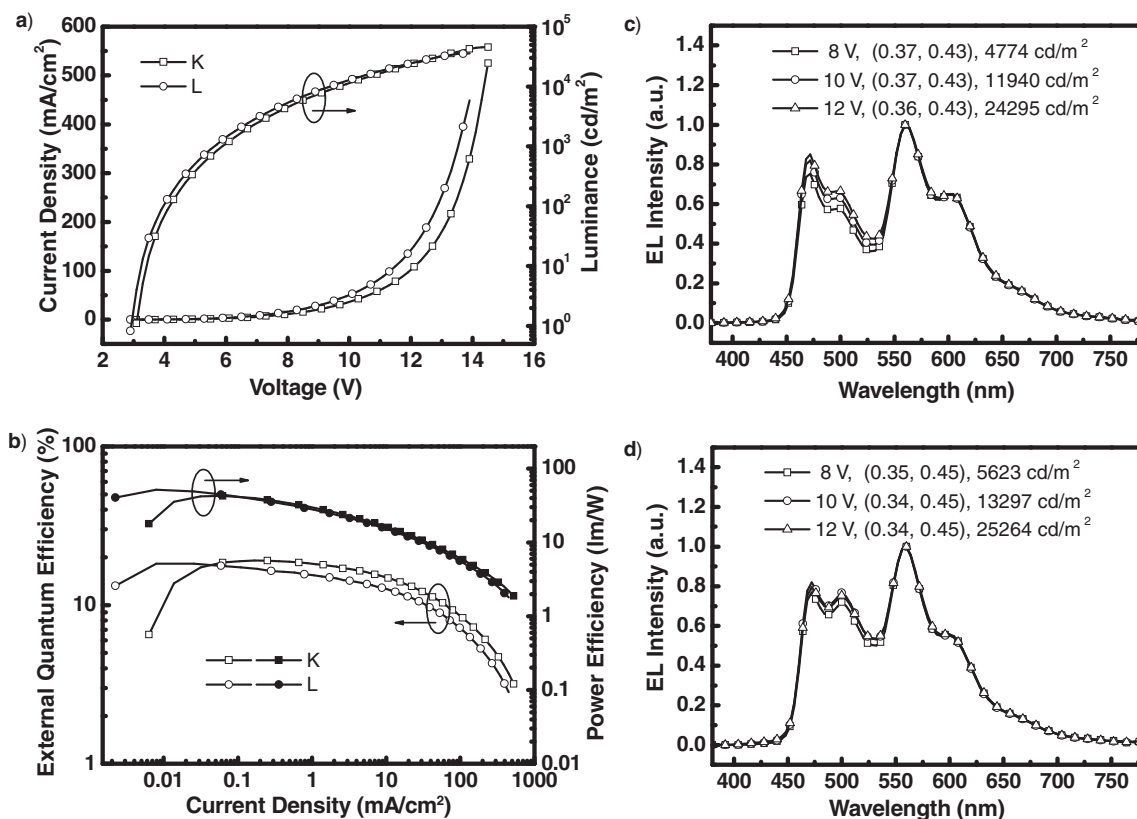


**Figure 11.** a) Current density-voltage-brightness characteristics for devices K and L. b) External quantum efficiency and power efficiency versus current density curves for devices K and L. c) The normalized EL spectra of device K at various voltages. d) The normalized EL spectra of device L at various voltages.

## 4. Experimental Section

**General Information:** <sup>1</sup>H NMR and <sup>13</sup>C NMR spectra were measured on a MECUYR-VX300 spectrometer. Elemental analyses of carbon, hydrogen, and nitrogen were performed on a Vario EL III microanalyzer. LC-Mass spectra were measured on a Waters ZQ-Mass ESI. UV-Vis absorption spectra were recorded on a Shimadzu UV-2500 recording spectrophotometer. PL spectra were recorded on a Hitachi F-4500 fluorescence spectrophotometer. Differential scanning calorimetry (DSC) was performed on a NETZSCH DSC 200 PC unit at a heating rate of 10 °C min<sup>-1</sup> from 20 to 300 °C under argon. The glass transition temperature (*T*<sub>g</sub>) was determined from the second heating scan. Thermogravimetric analysis (TGA) was undertaken with a NETZSCH STA 449C instrument. The thermal stability of the samples under a nitrogen atmosphere was determined by measuring their weight loss while heating at a rate of 10 °C min<sup>-1</sup> from 25 to 800 °C. Cyclic voltammetry (CV) was carried out in nitrogen-purged dichloromethane (oxidation scan) at room temperature with a CHI voltammetric analyzer. Tetrabutylammonium hexafluorophosphate (TBAPF<sub>6</sub>) (0.1 M) was used as the supporting electrolyte. The conventional three-electrode configuration consists of a platinum working electrode, a platinum wire auxiliary electrode, and an Ag wire pseudo-reference electrode with ferrocenium-ferrocene (Fc<sup>+</sup>/Fc) as the internal standard. Cyclic voltammograms were obtained at scan rate of 100 mV s<sup>-1</sup>. The onset potential was determined from the intersection of two tangents drawn at the rising and background current of the cyclic voltammogram.

**Computational Details:** The geometrical and electronic properties were performed with the Gaussian 09 program package.<sup>[27]</sup> The calculation was optimized by means of the B3LYP (Becke three parameters hybrid functional with Lee-Yang-Perdew correlation functionals)<sup>[28]</sup> with

the 6-31G(d) atomic basis set. Then the electronic structures were calculated at  $\tau$ -HCTHhyb/6-311++G(d, p) level.<sup>[29]</sup> Molecular orbitals were visualized using Gaussview.

**Device Fabrication and Measurement:** The hole-injection material MoO<sub>3</sub>, hole-transporting material 1,4-bis[(1-naphthylphenyl)amino]biphenyl (NPB), electron/exciton-blocking material 4,4',4''-tri(*N*-carbazolyl)triphenylamine (TCTA), and electron-transporting material 1,3,5-tris(*N*-phenylbenzimidazol-2-yl)benzene (TPBI) were commercially available. Commercial ITO (indium tin oxide) coated glass with sheet resistance of 10 Ω per square was used as the starting substrates. Before device fabrication, the ITO glass substrates were pre-cleaned carefully and treated by oxygen plasma for 2 min. Then the sample was transferred to the deposition system. MoO<sub>3</sub> (10 nm) was firstly deposited to ITO substrate, followed by NPB (80 nm), TCTA (5 nm), emissive layer, and TPBI (40 nm). Finally, a cathode composed of lithium fluoride (1 nm) and aluminum (100 nm) was sequentially deposited onto the substrate in the vacuum of 10<sup>-6</sup> Torr. The *L*-*V*-*J* of the devices was measured with a Keithley 2400 Source meter and a Keithley 2000 Source multimeter equipped with a calibrated silicon photodiode. The EL spectra were measured by JY SPEX CCD3000 spectrometer. The EQE values were calculated according to previously reported methods.<sup>[30]</sup> All measurements were carried out at room temperature under ambient conditions.

**Materials:** 2-{4-[(4-bromophenyl)(diphenyl)silyl]phenyl}-1-phenyl-1*H*-benzimidazole, 2-{3-[(3-bromophenyl)(diphenyl)silyl]phenyl}-1-phenyl-1*H*-benzimidazole, 2-{4-[(4-bromophenyl)(diphenyl)silyl]phenyl}-5-(4-*tert*-butylphenyl)-1,3,4-oxadiazole, 2-{3-[(3-bromophenyl)(diphenyl)silyl]phenyl}-5-(4-*tert*-butylphenyl)-1,3,4-oxadiazole were prepared according to previously reported procedures.<sup>[31]</sup>

(4-{diphenyl[4-(1-phenyl-1H-benzimidazol-2-yl)phenyl]silyl}phenyl)diphenylamine (1): A mixture of 2-[4-[(4-bromophenyl)(diphenyl)silyl]phenyl]-1-phenyl-1H-benzimidazole (1.82 g, 3.00 mmol), diphenylamine (0.54 g, 3.20 mmol), Pd(OAc)<sub>2</sub> (13 mg, 0.06 mmol), tBuONa (0.35 g, 3.60 mmol), (tBu)<sub>3</sub>PBF<sub>4</sub> (52 mg, 0.18 mmol), and toluene (20 mL) was refluxed under argon for 18 h. After cooling, the mixture was extracted with CH<sub>2</sub>Cl<sub>2</sub>, and the organic layer was dried over anhydrous Na<sub>2</sub>SO<sub>4</sub>. After removal of the solvent, the residue was purified by column chromatography on silica gel using ethyl acetate/petroleum (1:5 by vol.) as the eluent to give a white powder. Yield: 72%. <sup>1</sup>H NMR (300 MHz, CDCl<sub>3</sub>) δ [ppm]: 8.35 (d, J = 8.1 Hz, 1H), 7.80 (d, J = 8.1 Hz, 2H), 7.67–7.57 (m, 6H), 7.52–7.34 (m, 12H), 7.32–7.27 (m, 8H), 7.14 (d, J = 7.8 Hz, 4H), 7.07–7.00 (m, 4H). <sup>13</sup>C NMR (75 MHz, CDCl<sub>3</sub>) δ [ppm]: 152.28, 149.45, 147.52, 142.69, 137.52, 137.42, 137.16, 137.02, 136.63, 134.35, 130.74, 130.25, 129.93, 129.62, 129.06, 128.82, 128.17, 127.67, 125.44, 123.90, 123.77, 123.54, 121.75, 119.99, 110.84. MS (ESI): m/z 696 [M + H]<sup>+</sup>. Anal. calcd for C<sub>49</sub>H<sub>37</sub>N<sub>3</sub>Si (%): C 84.57, H 5.36, N 6.04; found: C 84.72, H 5.12, N 5.95.

(3-{diphenyl[3-(1-phenyl-1H-benzimidazol-2-yl)phenyl]silyl}phenyl)diphenylamine (2): 2 was prepared according to the same procedure as 1 but using 2-[3-[(3-bromophenyl)(diphenyl)silyl]phenyl]-1-phenyl-1H-benzimidazole. Yield: 74%. <sup>1</sup>H NMR (300 MHz, CDCl<sub>3</sub>) δ [ppm]: 7.86 (d, J = 7.5 Hz, 2H), 7.51–7.46 (m, 2H), 7.39–7.37 (m, 4H), 7.32–7.22 (m, 13H), 7.18–7.07 (m, 8H), 7.04 (d, J = 8.1 Hz, 4H), 6.97–6.91 (m, 4H). <sup>13</sup>C NMR (75 MHz, CDCl<sub>3</sub>) δ [ppm]: 153.10, 148.12, 147.79, 143.40, 137.86, 137.57, 137.50, 137.16, 136.80, 135.15, 134.95, 133.94, 132.19, 131.59, 131.03, 130.22, 130.11, 129.93, 129.71, 129.42, 128.78, 128.66, 128.39, 127.67, 125.75, 124.59, 123.92, 123.58, 123.26, 120.34, 111.02. MS (ESI): m/z 696 [M + H]<sup>+</sup>. Anal. calcd for C<sub>49</sub>H<sub>37</sub>N<sub>3</sub>Si (%): C 84.57, H 5.36, N 6.04; found: C 84.76, H 5.34, N 6.03.

{4-[[4-[5-(4-tert-butylphenyl)-1,3,4-oxadiazol-2-yl]phenyl]diphenyl]silyl}phenyl)diphenylamine (3): 3 was prepared according to the same procedure as 1 but using 2-[4-[(4-bromophenyl)(diphenyl)silyl]phenyl]-5-(4-tert-butylphenyl)-1,3,4-oxadiazole. Yield: 73%. <sup>1</sup>H NMR (300 MHz, CDCl<sub>3</sub>) δ [ppm]: 8.13 (d, J = 7.5 Hz, 2H), 8.06 (d, J = 8.4 Hz, 2H), 7.75 (d, J = 8.1 Hz, 2H), 7.60–7.54 (m, 6H), 7.46–7.38 (m, 8H), 7.30–7.25 (m, 4H), 7.15 (d, J = 7.8 Hz, 4H), 7.06–7.03 (m, 4H), 1.37 (s, 9H). <sup>13</sup>C NMR (75 MHz, CDCl<sub>3</sub>) δ [ppm]: 164.60, 164.27, 155.26, 149.19, 147.08, 139.67, 137.10, 136.80, 136.19, 133.68, 129.69, 129.23, 127.88, 126.66, 125.96, 125.81, 125.08, 124.65, 123.43, 121.35, 120.96, 34.97, 31.00. MS (ESI): m/z 704 [M + H]<sup>+</sup>. Anal. calcd for C<sub>48</sub>H<sub>41</sub>N<sub>3</sub>Osi (%): C 81.90, H 5.87, N 5.97; found: C 82.11, H 5.73, N 5.86.

{3-[[3-[5-(4-tert-butylphenyl)-1,3,4-oxadiazol-2-yl]phenyl]diphenyl]silyl}phenyl)diphenylamine (4): 4 was prepared according to the same procedure as 1 but using 2-[3-[(3-bromophenyl)(diphenyl)silyl]phenyl]-5-(4-tert-butylphenyl)-1,3,4-oxadiazole. Yield: 80%. <sup>1</sup>H NMR (300 MHz, CDCl<sub>3</sub>) δ [ppm]: 8.26 (s, 1H), 8.18 (d, J = 7.8 Hz, 1H), 8.00 (d, J = 8.1 Hz, 2H), 7.67 (d, J = 7.2 Hz, 1H), 7.55–7.35 (m, 14H), 7.30–7.25 (m, 2H), 7.17–7.15 (m, 5H), 7.07 (d, J = 7.8 Hz, 4H), 6.97–6.92 (m, 2H), 1.36 (s, 9H). <sup>13</sup>C NMR (75 MHz, CDCl<sub>3</sub>) δ [ppm]: 164.96, 164.72, 155.62, 147.84, 147.81, 139.78, 136.72, 136.63, 136.33, 134.67, 134.64, 133.55, 131.74, 130.62, 130.22, 129.52, 129.36, 128.86, 128.37, 127.10, 126.40, 125.42, 124.55, 123.93, 123.13, 121.40, 35.41, 31.48. MS (ESI): m/z 704 [M + H]<sup>+</sup>. Anal. calcd for C<sub>48</sub>H<sub>41</sub>N<sub>3</sub>Osi (%): C 81.90, H 5.87, N 5.97; found: C 82.28, H 5.65, N 6.06.

## Supporting Information

Supporting Information is available from the Wiley Online Library or from the author.

## Acknowledgements

We thank the National Natural Science Foundation of China (Project Nos. 90922020 and 50773057), the National Basic Research Program

of China (973 Program 2009CB623602 and 2009CB930603), the Open Research Fund of State Key Laboratory of Polymer Physics and Chemistry, Changchun Institute of Applied Chemistry, Chinese Academy of Sciences, and the Fundamental Research Funds for the Central Universities of China for financial support.

Received: September 30, 2010

Revised: November 21, 2010

Published online: February 10, 2011

- [1] M. A. Baldo, D. F. O'Brien, Y. You, A. Shoustikov, S. Sibley, M. E. Thompson, S. R. Forrest, *Nature* **1998**, *395*, 151.
- [2] a) M. A. Baldo, S. Lamansky, P. E. Burrows, M. E. Thompson, S. R. Forrest, *Appl. Phys. Lett.* **1999**, *75*, 4; b) X. Yang, D. Neher, in *Organic Light Emitting Devices* (Eds.: K. Müllen, U. Scherf), Wiley-VCH, Weinheim, **2006**, pp. 333–367.
- [3] a) A. Köhler, J. Wilson, R. Friend, *Adv. Mater.* **2002**, *14*, 701; b) T. Tsuzuki, S. Tokito, *Adv. Mater.* **2007**, *19*, 276; c) S.-J. Su, E. Gonmori, H. Sasabe, J. Kido, *Adv. Mater.* **2008**, *20*, 4189.
- [4] a) H. Sasabe, T. Chiba, S.-J. Su, Y.-J. Pu, K.-I. Nakayama, J. Kido, *Chem. Commun.* **2008**, 5821; b) Y. Tao, Q. Wang, C. Yang, C. Zhong, K. Zhang, J. Qin, D. Ma, *Adv. Funct. Mater.* **2010**, *20*, 304.
- [5] a) C. Adachi, M. A. Baldo, M. E. Thompson, S. R. Forrest, *J. Appl. Phys.* **2001**, *90*, 5048; b) Y. Z. Li, W. J. Xu, G. Z. Ran, G. G. Qin, *Appl. Phys. Lett.* **2009**, *95*, 033307.
- [6] a) C.-H. Chien, F.-M. Hsu, C.-F. Shu, Y. Chi, *Org. Electron.* **2009**, *10*, 871; b) Y. Tao, Q. Wang, L. Ao, C. Zhong, J. Qin, C. Yang, D. Ma, *J. Mater. Chem.* **2010**, *20*, 1759.
- [7] M. A. Baldo, C. Adachi, S. R. Forrest, *Phys. Rev. B: Condens. Matter Mater. Phys.* **2000**, *62*, 10967.
- [8] a) A. B. Padmameruma, L. S. Sapochak, P. E. Burrows, *Chem. Mater.* **2006**, *18*, 2389; b) S.-J. Su, H. Sasabe, T. Takeda, J. Kido, *Chem. Mater.* **2008**, *20*, 1691.
- [9] a) R. J. Holmes, B. W. D'Andrade, S. R. Forrest, X. Ren, J. Li, M. E. Thompson, *Appl. Phys. Lett.* **2003**, *83*, 3818; b) Z. Q. Gao, M. Luo, X. H. Sun, H. L. Tam, M. S. Wong, B. X. Mi, P. F. Xia, K. W. Cheah, C. H. Chen, *Adv. Mater.* **2009**, *21*, 688.
- [10] a) S.-J. Yeh, M.-F. Wu, C.-T. Chen, Y.-H. Song, Y. Chi, M.-H. Ho, S.-F. Hsu, C. H. Chen, *Adv. Mater.* **2005**, *17*, 285; b) M.-H. Tsai, Y.-H. Hong, C.-H. Chang, H.-C. Su, C.-C. Wu, A. Matoliukstyte, J. Simokaitiene, S. Grigalevicius, J. V. Grazulevicius, C.-P. Hsu, *Adv. Mater.* **2007**, *19*, 862.
- [11] a) J. Ding, B. Zhang, J. Lü, Z. Xie, L. Wang, X. Jing, F. Wang, *Adv. Mater.* **2009**, *21*, 4983; b) S. Ye, Y. Liu, J. Chen, K. Lu, W. Wu, C. Du, Y. Liu, T. Wu, Z. Shuai, G. Yu, *Adv. Mater.* **2010**, *22*, 4167.
- [12] X. Ren, J. Li, R. J. Holmes, P. I. Djurovich, S. R. Forrest, M. E. Thompson, *Chem. Mater.* **2004**, *16*, 4743.
- [13] M.-H. Tsai, H.-W. Lin, H.-C. Su, T.-H. Ke, C.-c. Wu, F.-C. Fang, Y.-L. Liao, K.-T. Wong, C.-I. Wu, *Adv. Mater.* **2006**, *18*, 1216.
- [14] M.-F. Wu, S.-J. Yeh, C.-T. Chen, H. Murayama, T. Tsuboi, W.-S. Li, I. Chao, S.-W. Liu, J.-K. Wang, *Adv. Funct. Mater.* **2007**, *17*, 1887.
- [15] a) Y. Tao, Q. Wang, C. Yang, Q. Wang, Z. Zhang, T. Zou, J. Qin, D. Ma, *Angew. Chem. Int. Ed.* **2008**, *47*, 8104; b) S.-y. Takizawa, V. A. Montes, P. Anzenbacher, Jr., *Chem. Mater.* **2009**, *21*, 2452.
- [16] a) F.-M. Hsu, C.-H. Chien, C.-F. Shu, C.-H. Lai, C.-C. Hsieh, K.-W. Wang, P.-T. Chou, *Adv. Funct. Mater.* **2009**, *19*, 2834; b) H.-H. Chou, C.-H. Cheng, *Adv. Mater.* **2010**, *22*, 2468.
- [17] J. F. Hartwig, *Acc. Chem. Res.* **1998**, *31*, 852.
- [18] a) C.-H. Chen, W.-S. Huang, M.-Y. Lai, W.-C. Tsao, J. T. Lin, Y.-H. Wu, T.-H. Ke, L.-Y. Chen, C.-C. Wu, *Adv. Funct. Mater.* **2009**, *19*, 2661; b) Y. Tao, Q. Wang, Y. Shang, C. Yang, L. Ao, J. Qin, D. Ma, Z. Shuai, *Chem. Commun.* **2009**, 77.
- [19] D.-R. Bai, X.-Y. Liu, S. Wang, *Chem. Eur. J.* **2007**, *13*, 5713.

- [20] R. J. Holmes, S. R. Forrest, Y. J. Tung, R. C. Kwong, J. J. Brown, S. Garon, M. E. Thompson, *Appl. Phys. Lett.* **2003**, *82*, 2422.
- [21] P.-I. Shih, C.-H. Chien, F.-I. Wu, C.-F. Shu, *Adv. Funct. Mater.* **2007**, *17*, 3514.
- [22] M. E. Kondakova, T. D. Pawlik, R. H. Young, D. J. Giesen, D. Y. Kondakov, C. T. Brown, J. C. Deaton, J. R. Lenhard, K. P. Klubek, *J. Appl. Phys.* **2008**, *104*, 094501.
- [23] Z. Ge, T. Hayakawa, S. Ando, M. Ueda, T. Akiike, H. Miyamoto, T. Kajita, M.-a. Kakimoto, *Adv. Funct. Mater.* **2008**, *18*, 584.
- [24] a) S. O. Jeon, K. S. Yook, C. W. Joo, J. Y. Lee, *Appl. Phys. Lett.* **2009**, *94*, 013301; b) J. Lee, J.-I. Lee, J. Y. Lee, H. Y. Chu, *Org. Electron.* **2009**, *10*, 1529.
- [25] a) C.-L. Ho, W.-Y. Wong, Q. Wang, D. Ma, L. Wang, Z. Lin, *Adv. Funct. Mater.* **2008**, *18*, 928; b) Y. Tao, Q. Wang, C. Yang, C. Zhong, J. Qin, D. Ma, *Adv. Funct. Mater.* **2010**, *20*, 2923.
- [26] a) J. Lee, J.-I. Lee, J. Y. Lee, H. Y. Chu, *Appl. Phys. Lett.* **2009**, *94*, 193305; b) Q. Wang, J. Ding, D. Ma, Y. Cheng, L. Wang, X. Jing, F. Wang, *Adv. Funct. Mater.* **2009**, *19*, 84.
- [27] Gaussian 09, Revision A.01, M. J. Frisch, G. W. Trucks, H. B. Schlegel, G. E. Scuseria, M. A. Robb, J. R. Cheeseman, G. Scalmani, V. Barone, B. Mennucci, G. A. Petersson, H. Nakatsuji, M. Caricato, X. Li, H. P. Hratchian, A. F. Izmaylov, J. Bloino, G. Zheng, J. L. Sonnenberg, M. Hada, M. Ehara, K. Toyota, R. Fukuda, J. Hasegawa, M. Ishida, T. Nakajima, Y. Honda, O. Kitao, H. Nakai, T. Vreven, J. A. Montgomery, Jr., J. E. Peralta, F. Ogliaro, M. Bearpark, J. J. Heyd, E. Brothers, K. N. Kudin, V. N. Staroverov, R. Kobayashi, J. Normand, K. Raghavachari, A. Rendell, J. C. Burant, S. S. Iyengar, J. Tomasi, M. Cossi, N. Rega, J. M. Millam, M. Klene, J. E. Knox, J. B. Cross, V. Bakken, C. Adamo, J. Jaramillo, R. Gomperts, R. E. Stratmann, O. Yazyev, A. J. Austin, R. Cammi, C. Pomelli, J. W. Ochterski, R. L. Martin, K. Morokuma, V. G. Zakrzewski, G. A. Voth, P. Salvador, J. J. Dannenberg, S. Dapprich, A. D. Daniels, O. Farkas, J. B. Foresman, J. V. Ortiz, J. Cioslowski, D. J. Fox, Gaussian Inc., Wallingford CT, **2009**.
- [28] a) A. D. Becke, *Phys. Rev. A* **1988**, *38*, 3098; b) C. Lee, W. Yang, R. G. Parr, *Phys. Rev. B* **1988**, *37*, 785.
- [29] A. D. Boese, N. C. Handy, *J. Chem. Phys.* **2002**, *116*, 9559.
- [30] S. R. Forrest, D. D. C. Bradley, M. E. Thompson, *Adv. Mater.* **2003**, *15*, 1043.
- [31] a) Z. Ge, T. Hayakawa, S. Ando, M. Ueda, T. Akiike, H. Miyamoto, T. Kajita, M.-a. Kakimoto, *Chem. Mater.* **2008**, *20*, 2532; b) X. Zheng, Z. Li, Y. Wang, W. Chen, Q. Huang, C. Liu, G. Song, *J. Fluorine Chem.* **2003**, *123*, 163.